Published in final edited form as:
Nat Chem. 2014 March ; 6(3): 208–215. doi:10.1038/nchem.1868.

Ion Mobility Mass Spectrometry of a Rotary ATPase Reveals ATP-induced Reduction in Conformational Flexibility

Min Zhou[#1], **Argyris Politis**[#1], **Roberta Davies**[2,3], **Idlir Liko**[1], **Kuan-Jung Wu**[1], **Alastair G. Stewart**[2,3], **Daniela Stock**[2,3], and **Carol V. Robinson**[1]

[1]Department of Chemistry, Physical and Theoretical Chemistry Laboratory, University of Oxford, Oxford OX1 3QZ, UK

[2]The Victor Chang Cardiac Research Institute, Darlinghurst NSW 2010, Australia

[3]The University of New South Wales, Sydney NSW 2052, Australia

[#] These authors contributed equally to this work.

Abstract

Rotary ATPases play fundamental roles in energy conversion, their catalytic rotation being associated with inter-domain fluctuations and heterogeneity of conformational states. Using ion mobility mass spectrometry (IM-MS) we compare the conformational dynamics of the intact ATPase from *Thermus thermophilus* (*Tt*ATPase) with its membrane and soluble subcomplexes. Our results define regions with enhanced flexibility assigned to distinct subunits within the overall assembly. To provide a structural context for our experimental data we performed molecular dynamics (MD) simulations and observed conformational changes of the peripheral stalks reflecting their intrinsic flexibility. By isolating complexes at different phases of cell growth and manipulating nucleotides, metal ions and pH during isolation, we reveal differences that can be related to conformational changes in the V_o complex, triggered by ATP binding. Together these results implicate nucleotides in modulating flexibility of the stator components and uncover mechanistic detail underlying operation and regulation in the context of the holo-enzyme.

Rotary ATPases are highly efficient molecular nanomotors essential to biological energy metabolism. Classified into three subtypes F-, V- and A-type (also referred to as prokaryotic V-type), they share a conserved architecture comprising a water-soluble catalytic head and a membrane-embedded base, termed V_1 and V_o in *Tt*ATPase, respectively[1,2]. *Tt*ATPase is the only ATPase in *Thermus thermophilus* and can operate in two directions towards ATP production or proton pumping depending on cellular requirements[3,4]. ATP synthesis/hydrolysis occurs in V_1 and is coupled to H^+/Na^+ translocation in the membranous V_o via a rotational motion of the subunits D, F, C anchored to a membrane embedded ring (the rotor). The remaining subunits constitute the stator including the AB hexamer and peripheral stalks

To whom correspondence should be addressed: carol.robinson@chem.ox.ac.uk or min.zhou@chem.ox.ac.uk.
Author contributions C.V.R. and D.S designed the research; M.Z. conducted all IM-MS experiments and analysed the data; R.D. purified *Tt*ATPases; A.P. and A.S. performed modelling; A.P. conducted MD simulation and all CCS calculations; I.L. did MS analysis of dAb:*Tt*ATPase binding; K.J.W. conducted the Western blot experiments; M.Z. and C.V.R wrote the paper.

Competing Financial Interests statement The authors declare no competing financial interests.

Europe PMC Funders Author Manuscripts

in V_1 that connect to subunit I in V_o. A wealth of structural information is available for individual components of V_1, whereas the membranous V_o and intact V_1V_o complex resist high-resolution structural elucidation[1,5]. The difficulty arises in part from the flexibility required for the synergetic cooperation of components from both soluble and membrane domains, resulting in heterogeneity of conformational states along the time axis of rotary catalysis. This combined with the amphipathic nature and dynamic disassembly[6,7] of intact complexes presents significant challenges for traditional structural biology approaches.

Recent discovery of conditions for the introduction of membrane-embedded assemblies into the gas phase and its coupling with ion mobility mass spectrometry (IM-MS) has enabled conformation and dynamics of membrane proteins to be assessed. The method exploits the protective effect of detergent micelles during transfer and gas phase excitation to release complexes from detergent encapsulation[8,9] enabling native-like structures to be retained[10,11]. This implies that collision energy is directed primarily towards disruption of detergent assemblies without perturbing the structures of membrane complexes.

IM separation is based on the ability of ions to traverse a gas-filled chamber under the influence of an electric field[12]. Ions of different size and shape experience different resistance along their migration colliding with inert gas molecules[13,14,15]; their arrival time distributions (ATD) are recorded and converted to orientationally averaged collision cross sections (CCS)[16,17]. Experimental CCSs can be used as restraints to guide structural modelling of protein complexes[18,19]. ATD peaks are generally Gaussian but for complexes in which unfolding occurs, asymmetric peaks, skewed towards slower arrival times, are observed[17,20]. Structural dynamics and heterogeneity can be inferred from the distribution of mobilities; ions with multiple conformations resulting in broad Gaussian shaped ATD peaks[10,15].

Recently we demonstrated that two prokaryotic V-type ATPases, encapsulated in detergent micelles, could be projected into the vacuum of a mass spectrometer. Release of “naked” ions by collisional excitation enabled us to explore their subunit interactions, lipid binding properties and the structural consequence of nucleotide binding[21]. Here we extend our study using IM-MS to characterise the 3D topology of *Tt*ATPase. We show that native-like structure can be preserved in vacuum and contrast variation in CCS of the intact complex with different subcomplexes enabling us to assign dynamics to the peripheral stalks, in accord with MD simulations. By exploring *in vivo* and *in vitro* conditions we reveal conformational changes in V_o triggered by ATP binding. Collectively these results relate nucleotide binding to stability and link conformational flexibility to cellular ATP/ADP levels.

Results

*Tt*AtPase (V_1V_o) emerges from detergent micelles without major structural distortion

To assess the overall topology in the absence of bulk membrane lipids or detergents we acquired IMMS spectra for intact *Tt*ATPase (Fig. 1). Under carefully controlled conditions three charge state series were recorded and assigned to intact V_1V_o, disassembled V_1 (A_3B_3DF) and membranous V_o (ICL_{12}). Reduction in charge was observed for species

containing transmembrane regions (V_1V_o and V_o, Supplementary Table S1), consistent with reduced accessible surfaces due to the presence of detergent micelles[22,23]. ATDs recorded for all three species are well-defined Gaussians implying that they emerge from detergent micelles without major structural distortion.

To correlate IM data with solution phase structures, centroids were extracted from the IM peaks and calibrated against a CCS database of proteins and protein complexes[24]. Experimental CCS were compared with theoretical values calculated for structures assembled by docking, homology and coarse-grained modelling, guided by the EM density map (Supplementary Methods). Good agreement was observed for all three species V_1, V_o and intact V_1V_o (Table 1, all within 1.0%) implying that the conformations of these complexes in the gas phase do not deviate significantly from their anticipated structures.

Intact V_1V_o, V_1 and V_o sub-domains display markedly different IM arrival time distributions

We noticed that the three species V_1, V_o and V_1V_o within the same IM-MS spectrum display well-resolved Gaussian peaks but have markedly different widths (Fig. 1 (i-iii)). In comparison to the intact V_1V_o, ATDs recorded for V_1 (A_3B_3DF) are much narrower while for V_o (ICL_{12}) much broader ATDs are observed. We computed average arrival time resolution (R_t), expressed as $t/\Delta t$, which is affected by experimental conditions and dictated primarily by diffusion of ions through the IM chamber[25,26]. It is expected that theoretical R_t values for V_1, V_o and V_1V_o should remain steady (estimated 12% lower for V_o and 5% higher for V_oV_1 *cf.* V_1, Supplementary Methods). R_t values measured experimentally however span a much wider range (70% and 44% lower for V_o and V_oV_1 respectively than V_1, Table 1).

Since R_t is both instrument and ion-dependent we converted R_t values to R_Ω (centroid CCS normalised to width at half-height). IM peaks assigned to V_1 are sharp with an average R_Ω of 34.6 corresponding to a CCS variation of 2.9%, close to the limiting resolution of the instrumentation employed[25,27], implying that V_1 exists in one principal conformation similar to the X-ray structure[28]. By contrast V_o has a much lower R_Ω (10.8) consistent with its CCS span being three-fold greater than V_1 (9.2% *vs.* 2.9%, Table 1). This broadening likely reflects heterogeneity characteristic of an ensemble of conformations populated by V_o.

Reduced flexibility of V_o was attributed to ATP binding to the membrane subunit I

To investigate the origin of this conformational heterogeneity we explored a series of *in vivo* and *in vitro* conditions, monitoring their effects on the structural dynamics of V_o. Conditions included: (i) harvesting cells at nutrient-abundant *vs.* nutrient-limited status; (ii) pH manipulation (6.8 or 8.2); (iii) use of chelating EDTA to sequester metal ions; and (iv) ATP or AMPPNP supplement to purification buffers, leading to 12 different purifications (Table 3). Results showed that cellular nutrition status, pH, metal ions or AMPPNP had no appreciable effect on the CCS of V_o (Table 2). By contrast, ATD peaks recorded for V_o in all preparations supplemented with 1mM ATP shifted to shorter drift times, indicative of an average structural compaction of 146 $Å^2$ (Fig. 2a, left panel). This CCS reduction was observed for all ATP-supplemented preparations with reproducibility (Fig. 2b & 2c), and

was invariably accompanied by a narrower mobility distribution (higher R_Ω, Table 2). Our IM data therefore point to a compact, defined structure of V_o induced by ATP binding.

To identify the cause of this structural compaction we performed in-solution disassembly of V_o (ICL_{12}) generating CL_{12} from loss of subunit I. CL_{12} exhibited much narrower CCS distributions than ICL_{12}, with a CCS close to that calculated from the modelled structure (Fig. 2a, right panel) allowing us to assign conformational heterogeneity to subunit I. Moreover lack of ATP-associated changes of IM profiles for CL_{12} further pinpointed subunit I as being responsible for ATP-induced compaction and reduction in dynamics of V_o. Therefore in preparations lacking ATP the broad ATD peaks of V_o are associated with dynamics of subunit I, while ATP not only reduces the CCS of V_o by *ca.* 146 $Å^2$ but also narrows the distribution from 9 to 6% (Table 2).

To account for the CCS difference of V_o in the presence and absence of ATP, we built a structural model of V_o reproducing its conformation within intact *Tt*ATPase (Supplementary Methods), in which the soluble portion of I (I_{sol}) runs parallel to the membrane plane and forms a ~90° angle with its membrane domain (I_{mem}) (Fig. 2 (vi)). Theoretical CCS estimated for this model agrees well with measured value of V_o in the presence of ATP. In its absence the observed CCS of V_o increases implying deviation of I_{sol} from its original conformation. To estimate the conformational flexibility of subunit I we performed normal mode analysis (NMA)[29] computing the low frequency modes of I_{sol}, employing the crystal structure of the yeast analogue of I_{sol} (subunit C, PDB code: 1U7L)[30]. NMA established elasticity in the long α-helical region in the middle part of the structure. This allowed the distal end of I_{sol} to flex upward with an offset of 10 Å and a 15° angle, resulting in an alternative conformation that we referred to as I_{sol}' (Supplementary Fig. S2). Incorporating this elasticity into the model of V_o led to a predicted CCS difference of 137 $Å^2$ (Fig. 2, (iii) *vs.* (vi)), in line with the CCS deviation observed experimentally (Table 2, 146 $Å^2$). Interestingly I_{sol}' produced by NMA mirrors a second structure of subunit C solved at 2.9 Å[30].

To correlate CCS distributions of V_o with conformational dynamics we generated a series of structural models for V_o incorporating I_{sol} or I_{sol}', varying the angle with I_{mem} in 5° increments, from 80° up to 150°. Theoretical CCSs were calculated and compared with experimental values, enabling us to estimate an angular freedom for I_{sol} in the presence of ATP of *ca.* 30° (80° to 110°, Supplementary Table 3). By contrast absence of ATP caused I_{sol}' to have enhanced angular freedom *ca.* 60° (80° to 140°) (Fig. 2d & 2e). Taken together these results highlight a nucleotide-induced change in the dynamics of subunit I in the isolated V_o complex.

Conformational diversity of V_1V_o is caused by "wobbling" of the catalytic head

This dynamic motion of subunit I, with and without ATP, would likely be restrained within the intact V_1V_o complex by interaction with the peripheral EG stalks[31,32]. Interestingly ATD peaks recorded for intact V_oV_1 are less broad than those of V_o (R_Ω 18.5 *vs.* 10.8 respectively, Table 1), suggesting a smaller conformational space occupied by V_1V_o. Since both complexes contain subunit I this implies that its conformational dynamics observed in ICL_{12} are restrained in the intact assembly. However, even with the movement of I

constrained it is not possible to achieve similar IM resolution for V_oV_1 to that of V_1 (R_Ω 18.5 *vs.* 34.6) implying that residual dynamics remains for V_oV_1.

We considered the characteristic "wobbling"[33,34] of the catalytic head, consistent with inclination of V_1 relative to V_o, to estimate the CCS variation for the intact complex. Taking into account rotation of the central stalk, and flexing of both peripheral stalks adopting alternative conformations during rotation, a theoretical CCS difference of 3.7% was anticipated (Supplementary Table S4). A variation of 5.4 ± 0.9% was measured by IM (Table 1, see below, Fig. 4a). This conformational broadening, when the motion of subunit I is restrained, mirrors an ensemble of coexisting structures of the intact *Tt*ATPase, possibly trapped at different stages along the dynamic process of rotary catalysis.

To support this proposal we probed the dynamic nature of the intact complex using an antibody (dAb) that recognises the EG stalks with high specificity[35]. MS spectra recorded for V_1V_o following incubation with a large excess of dAb reveal sub-stoichiometric binding, implicating different affinities of the two EG stalks in binding dAb (Supplementary Methods). We interpret this as evidence for a conformational divergence associated with the EG stalks, in accord with their role in accommodating the wobbling rotation of the asymmetrical complex.

Conformational broadening of V_1' can be assigned to dynamics of the EG stalks

Next we turned our attention to the isolated V_1 subcomplex, formed by loss of both peripheral stalks as well as the membrane V_o complex. Sharp ATDs were observed consistent with minimal variation in CCS for V_1 (R_Ω = 34.6, Table 1). This illustrates uniformity of conformations, in keeping with the 3-fold symmetry of V_1 around the central axis perpendicular to the A_3B_3 plane (Fig. 1(ii)); structures of V_1 after rotation of the central stalk by 0, 120 and 240° are superimposable. Conformational fluctuation associated with intermediate states however cannot be ruled out[36] but likely occurs on a minor scale since they are not detected with our IM instrumentation[25,37]. We conclude that the soluble head, in the absence of the peripheral stalks, exhibits the least conformational heterogeneity.

Disassembly of the intact complex in solution leads to the V_1' assembly with two peripheral stalks attached. IM data of V_1' give an experimental CCS of 172 nm^2 (Fig. 1 right), *cf.* 173 nm^2 calculated for V_1' assembled by docking the peripheral stalks onto V_1 (Table 1, SI). Overlapping peaks of low intensity around 9,000 m/*z* arise primarily from loss of both stalks as well as one B subunit (A_3B_2DF, Fig. 1 (v), Supplementary Table S1). Comparing the IM peak widths recorded for V_1' with those of A_3B_2DF, generated in the same solution and subject to the same MS conditions (Table 1), clearly demonstrates a conformational diversity for V_1', not present in A_3B_2DF, assigned to the binding of the peripheral stalks.

The peripheral EG stalk features a coiled coil tail extruding 120 Å from the main structure[31] (Fig. 1 (iv)). The close correlation of the CCS measurement with the native topology of V_1', as well as significant structural heterogeneity demonstrated for the assembly (Table 1) is in contrast to a previous IM-MS study which revealed collapse of intrinsically disordered loops onto a folded "core"[38]. To explore the gas phase behaviour of V_1' we carried out *in vacuo* MD simulations (Fig. 3). Interestingly no collapse of peripheral stalks was observed during

the course of simulations (1 nanosecond). On the contrary, MD simulations illustrated remarkable flexibility of distal ends of the stalks, while the globular domains, anchored to the catalytic head (V_1), remained essentially unaltered.

It is interesting to consider flexibility of V_1' in the light of distinct structures of the *T. thermuphilus* peripheral stalks reported recently[31,33]. Models of V_1' incorporating combinations of these structures and their inter-conversion, give a calculated CCS difference of up to 1026 Å^2 (Fig. 3c & S3). Selecting two V_1' models that yield the largest CCS difference and comparing their MD simulations (Fig. 3a & b, movie S1 & 2) initially for both models we observe conformational fluctuations, which start to stabilise after *ca.* 0.2 ns. Comparing CCS changes over the second 0.5 ns period of both simulations we obtain a theoretical value of 4.5%.

To compare this theoretical variation with the value established experimentally for V_1' (7.0±1.0%, Table 1), we considered all four species with conformational heterogeneity investigated here (V_o, V_1' V_1 and A_3B_2DF) and plotted their theoretical CCS variations against experimental values (Fig. 4a). An excellent linear correlation was found for two datasets with a positive y-interception of >2.0%, close to the limit set by the current IM approach[25]. The close correlation therefore verifies our conclusion of increased conformational flexibility assigned to the peripheral stalks during rotary catalysis, a mechanism that accommodates "wobbling" of the catalytic head.

Discussion

Here we report an in-depth IM-MS investigation of the intact *Tt*ATPase and demonstrate that it is possible to retain the structural integrity of this rotary enzyme and its subcomplexes, in the absence of bulk solvent and detergent. We show that the broad ATD pattern for V_o is attributed to flexibility of subunit I, and demonstrate compaction and reduction in dynamics in the presence of ATP. We also provide experimental evidence for flexibility of the EG stalks, closely reflected by MD simulations. Incorporation of this flexibility enabled us to assess the scope of conformational change for the intact ATPase during rotary catalysis, and more importantly, to explore a nucleotide regulatory mechanism of the complex responding to unfavourable cellular conditions, similar to the reversible disassembly established in eukaryotic V-ATPases (Fig. 4b).

Although the catalytic and regulatory roles of nucleotides in the hydrophilic V_1-headpiece have been established[28,36], their binding in the membranous V_o are less well-understood. Nucleotide-binding capabilities however have been reported for the C subunits of *S. cerevisiae* and *A. thaliana* V_1V_o[39], functional analogues of I_{sol} in *Tt*ATPase[6]. Accordingly lack of ATP was proposed to promote disassembly of isolated V_o domain of *Tt*ATPase[21]. Prompted by these initial observations here we carried out a systematic study assessing the role of a variety of factors on the conformational dynamics of isolated V_o. The study uncovered a role for ATP in stabilising the native conformation of I_{sol} restricting its mobility; depletion of ATP was shown not only to trigger a conformational change in I_{sol} converting to I_{sol}', but also to increase its freedom of movement from an angular range of 30° in the presence of ATP, to 50° in its absence.

Subunit I is the least understood yet evolutionarily conserved component across the ATPase family, for which no structural information is available. As the sole amphipathic protein of *Tt*ATPase its I_{sol} and I_{mem} domains, connected by an intermediate 'hinge' region[21,39], tether the EG stalks and constitute the proton channel across the membrane, respectively. Elasticity of the hinge region is obligatory to enable mobility of the periplasmic components without disrupting integrity of the transmembrane channel. Considering nucleotide-induced changes of V_o when ATP is supplemented, fluctuation of I_{sol} may well reflect elasticity of subunit I enabling dynamic movement of the catalytic head in a wobbling ATPase. Conversely when ATP is depleted our observation points to a mechanism of how cellular ATP levels are sensed and regulate the intact enzyme: in lack of ATP, ADP (or other nucleotides) likely competes for binding in the hinge domain of I and induces a conformational change converting I_{sol} to I_{sol}'. Optimal interaction of subunit I formed with the EG stalks is therefore compromised resulting in a strained complex of reduced stability, prone to disassemble into V_o and V_1. Once separated, increased mobility of I_{sol} in V_o further destabilises interaction of I_{mem} with the rotor ring (CL_{12}) leading to dissociation of subunit I. The mechanism is underpinned by minimal contact observed between I and CL_{12} ring by EM[40], and is postulated as a means for silencing the proton translocating V_o detached from the intact complex[21].

We speculate that ATP could execute its effect through: (i) competing at higher concentration for the nucleotide binding site in the hinge region of I which preferentially binds ADP[21,39], hence preventing a conformational change and relaxation associated with ADP binding; (ii) transient binding to a different site enhancing conformational stability of V_o. Either way our observations suggest a generality of nucleotide-induced conformational changes in the stator connecting the cytoplasmic V_1 and membranous V_o domains. Cellular ATP concentration is typically 1–10 mM[41]; the available ATP pool is expected to be in the sub-millimolar range given its association with the many molecular machineries involved in a multitude of energy-dependent processes[42]. Our results therefore bear physiological implications for the *in vivo* control mechanism via ATP/ADP ratios by showing a stabilisation by 1mM ATP while an ADP concentration of > 50μM is sufficient for relaxation of V_o[21].

A characteristic feature of eukaryotic V-type ATPases is the regulatory reversible disassembly of V_1 and V_o domains[5]. By demonstrating the dynamic properties of the EG stalks and subunit I in isolated V_1 and V_o of *Tt*ATPase respectively, our IM-MS data point to a critical role of the stator components in maintaining stability of intact V_oV_1. Peripheral stator components impart characteristics unique to V-ATPases; they must balance the stability essential for productive catalysis with the dynamic instability involved in regulation. Our results therefore raise the intriguing possibility of a reversible dissociation mechanism in analogy to eukaryotic V-type ATPases, likely mediated by the subunit I and peripheral stalks[43], in response to cellular ATP/ADP levels for the bacterium *Thermus thermophilus*. Binding of ATP favours the active conformation of I in V_1V_o maintaining an efficient ion pump. Conversely when ATP is depleted the complex reverts towards ATP synthesis; the integrity of which is maintained through a mechanism involving transmembrane proton motive force (PMF). Lack of both ATP and PMF (mimicking a

nutrient-deprived state) leads to conformational changes associated with increased dynamics induced by ADP binding in I_{sol} perturbing its optimal binding with the EG stalks, serving to initiate the cooperative "unloading" of V_1 from V_o. In this regard it is of interest to consider an early result which showed binding of *S. cerevisiae* C subunit (I_{sol} analogue) to the *M. Sexta* V_1 lacking endogeneous subunit C (V_1-C) significantly enhanced its ATP hydrolysis[44], supporting the notion that restriction of the peripheral stalks is desirable for optimal ATPase activity.

High-resolution structural biology tools have generated an ever-increasing database of static structures; their dynamic conformations however are among the most difficult to assess despite the fact that these often underpin the function and regulation of macromolecular machineries. Here we have shown how distribution of ATD can be used to assess rotations and conformational fluctuations in membrane-embedded rotary motors. With the aid of structural modeling and *in vacuo* MD simulation we relate these distributions to conformational flexibility, essential for the cooperativity and regulation of the dynamic nanomotor. Plotting theoretical values against experimental data enables us to isolate conformational heterogeneity from a background of factors contributing to IM distributions. Overall our results not only allow elucidation of nucleotide regulated flexibility for the *Tt*ATPase, but also highlight the potential of IM-MS to probe subtle conformational changes within membrane-embedded assemblies that often elude high-resolution structural characterisation due to averaging across populations of interconverting states.

Methods

Preparation of intact V_oV_1 complex and subcomplexes

Intact V_oV_1 was purified from *Thermus thermophilus* strain HB8 as previously described[32,35]. *Thermus thermophilus* cells were grown at 65°C (150 rpm) to stationary or log phase, and purified with supplements indicated in Table 3 (see SI for details). Purified V_oV_1 were buffer exchanged into 200mM AmAc and diluted to 1.1 mg/mL prior to IM-MS experiments. The CL_{12} subcomplex was generated by decreasing the pH[21], and disassembly to V_1' subcomplex was achieved *via* a further dilution (1:10) bringing the DDM concentration well below its critical micelle concentration (CMC) with IM-MS spectra immediately recorded.

Ion mobility mass spectrometry experiments

All IM-MS spectra were recorded on hybrid quadrupole (Q)-IM-ToF MS instruments known as Synapt[27] or Synapt G2[37] HDMS systems incorporating travelling-wave ion guide for IM separation (Waters, UK). Both instruments are modified for high mass[45] and use nitrogen as mobility gas with the trap and transfer regions filled with argon except for measurement of the intact V_oV_1 sulphur hexafluoride (SF6) was used. Instrument conditions were optimized for high m/*z* ions with acceleration kept minimal to avoid thermal heating of ions. Specifically ions were injected into the mobility cell at a 100 μs pulse with a voltage of 18V. The pressures of Synapt were maintained at $4.33e^{-1}$ and $3.42e^{-2}$ mbar in the mobility and trap/transfer regions, respectively. Triplicate measurements employing different combinations of wave height (WH) and wave velocity (WV) are listed (Supplementary

Table S2). The Synapt G2 system was operated at higher pressures of 3.25 and 3.95e^{-2} mbar for mobility and trap/transfer regions, respectively, which are separated by a 'helium gate' pressurized at 1.43 bar. Triplicate experiments were carried out with a fixed WH of 40V and varied WV at 550, 600 and 640ms^{-1} (Supplementary Table S2). Measurement of the disassembled V_1' was taken on the Synapt operated at 3.96e^{-1} and 5.93e^{-2} mbar for the mobility and trap/transfer regions, respectively. Mobility separations were performed with a fixed WV of 300ms^{-1} and varied WH at 8, 10 and 11V. CCS Measurement for the V_o (ICL_{12}) and CL_{12} subcomplexes was carried out on Synapt G2 maintaining 1.49 and 3.08e^{-2} mbar for mobility and trap/transfer regions, respectively, and helium gate pressurized at 9.66e^{-1} bar. Mobility separation was performed with a WH of 31V and WV of 800ms^{-1}. The Measurements were both replicated four times under identical instrumental conditions.

IM data analysis

Individual IM arrival time distributions (ATD) were extracted and converted to collision cross section (CCS) distributions using a calibration procedure described elsewhere[17], based on a set of proteins and protein complexes used as IM standards encompassing a wide mass range[24]. For each extracted ATD, arrival time resolution (R_t) was measured as the peak centroid divided by its width at 50% height ($t/\Delta t$). Similarly cross section resolution (R_Ω) was calculated as the centroid CCS value divided by the span of the CCS distribution at 50% height ($\Omega/\Delta\Omega$). The CCS variations are the average half-height spans of the CCS distributions normalized to their respective centroid CCSs. The R_t, R_Ω, experimental CCS and CCS variations reported in Table 1 are average values across each charge state series.

MD simulations

The simulations were performed in double floating-point precision with GROMACS 4.5.3 using the OPLS-AA/L force field[20,46]. The procedure started with a steepest descent energy minimization followed by 1 ns vacuum equilibration with randomly generated initial velocities. Neither periodicity nor cut-offs were employed in the calculations. Energy conservation was achieved using a 1 fs integration step, and constraining bonds to hydrogen with the LINCS algorithm[47]. A dielectric constant of $\varepsilon = 2\varepsilon_0$ (where ε_0 is the dielectric permittivity of free space) was used to describe the gas-phase basicity in our calculations[48]. The simulations were run at constant temperature of 300 K. To assign charged residues we employed an in-house developed search algorithm which evenly distributed charges over basic residues <5 Å from the surface[20]. Two alternative configurations were prepared for each complex, and three trajectories were analysed with respect to their RMSD from the initial structure. An RMSD-clustering algorithm was used to identify the most populated conformations at different stages in each trajectory, and CCSs were calculated for structures every 20 picoseconds (see SI for details).

Supplementary Material

Refer to Web version on PubMed Central for supplementary material.

Acknowledgments

This work has been funded by the Wellcome Trust (M.Z. and C.V.R.) and by the PROSPECTS (HEALTHF4-2008-201648) grant within the Research Framework of the European Union (A.P. and C.V.R.), together with EPSRC funding for research scientists with caring responsibilities (M.Z.), funding from the Royal Society and an ERC investigator award IMPRESS (C.V.R.). D.S., R.D., and A.G.S. are funded by Australian NH&MRC grants 1004620, 1022143 and 1047004, respectively.

References

1. von Ballmoos C, Cook GM, Dimroth P. Unique rotary ATP synthase and its biological diversity. Annu. Rev. Biophys. 2008; 37:43–64. [PubMed: 18573072]
2. Stewart AG, Sobti M, Harvey RP, Stock D. Rotary ATPases: models, machine elements and technical specifications. Bioarchitecture. 2013; 3(1):2–12. [PubMed: 23369889]
3. Nakano M, et al. ATP hydrolysis and synthesis of a rotary motor V-ATPase from Thermus thermophilus. J. Biol. Chem. 2008; 283(30):20789–20796. [PubMed: 18492667]
4. Feniouk BA, Suzuki T, Yoshida M. Regulatory interplay between proton motive force, ADP, phosphate, and subunit epsilon in bacterial ATP synthase. J. Biol. Chem. 2007; 282(1):764–772. [PubMed: 17092944]
5. Muench SP, Trinick J, Harrison MA. Structural divergence of the rotary ATPases. Q. Rev. Biophys. 2011; 44(3):311–356. [PubMed: 21426606]
6. Oot RA, Huang LS, Berry EA, Wilkens S. Crystal structure of the yeast vacuolar ATPase heterotrimeric EGC(head) peripheral stalk complex. Structure. 2012; 20(11):1881–1892. [PubMed: 23000382]
7. Yokoyama K, et al. Subunit arrangement in V-ATPase from Thermus thermophilus. J. Biol. Chem. 2003; 278(43):42686–42691. [PubMed: 12913005]
8. Barrera NP, et al. Mass spectrometry of membrane transporters reveals subunit stoichiometry and interactions. Nat. Methods. 2009; 6(8):585–587. [PubMed: 19578383]
9. Barrera NP, Di Bartolo N, Booth PJ, Robinson CV. Micelles protect membrane complexes from solution to vacuum. Science. 2008; 321(5886):243–246. [PubMed: 18556516]
10. Wang SC, et al. Ion mobility mass spectrometry of two tetrameric membrane protein complexes reveals compact structures and differences in stability and packing. J. Am. Chem. Soc. 2010; 132(44):15468–15470. [PubMed: 20949939]
11. Borysik AJ, Hewitt DJ, Robinson CV. Detergent release prolongs the lifetime of native-like membrane protein conformations in the gas-phase. J. Am. Chem. Soc. 2013; 135(16):6078–6083. [PubMed: 23521660]
12. Bohrer BC, Merenbloom SI, Koeniger SL, Hilderbrand AE, Clemmer DE. Biomolecule analysis by ion mobility spectrometry. Annu. Rev. Anal. Chem. 2008; 1:293–327.
13. Bleiholder C, Dupuis NF, Wyttenbach T, Bowers MT. Ion mobility-mass spectrometry reveals a conformational conversion from random assembly to beta-sheet in amyloid fibril formation. Nat. Chem. 2011; 3(2):172–177. [PubMed: 21258392]
14. Grabenauer M, et al. Conformational stability of Syrian hamster prion protein PrP(90-231). J. Am. Chem. Soc. 2010; 132(26):8816–8818. [PubMed: 20536231]
15. Dupuis NF, Wu C, Shea JE, Bowers MT. Human islet amyloid polypeptide monomers form ordered beta-hairpins: a possible direct amyloidogenic precursor. J. Am. Chem. Soc. 2009; 131(51):18283–18292. [PubMed: 19950949]
16. Michaelevski I, Kirshenbaum N, Sharon M. T-wave ion mobility-mass spectrometry: basic experimental procedures for protein complex analysis. J. Vis. Exp. 2010; (41)
17. Ruotolo BT, Benesch JL, Sandercock AM, Hyung SJ, Robinson CV. Ion mobility-mass spectrometry analysis of large protein complexes. Nat. Protoc. 2008; 3(7):1139–1152. [PubMed: 18600219]
18. Hall Z, Politis A, Robinson CV. Structural modeling of heteromeric protein complexes from disassembly pathways and ion mobility-mass spectrometry. Structure. 2012; 20(9):1596–1609. [PubMed: 22841294]

Europe PMC Funders Author Manuscripts

19. Alber F, et al. Determining the architectures of macromolecular assemblies. Nature. 2007; 450(7170):683–694. [PubMed: 18046405]
20. Hall Z, Politis A, Bush MF, Smith LJ, Robinson CV. Charge-state dependent compaction and dissociation of protein complexes: insights from ion mobility and molecular dynamics. J. Am. Chem. Soc. 2012; 134(7):3429–3438. [PubMed: 22280183]
21. Zhou M, et al. Mass spectrometry of intact V-type ATPases reveals bound lipids and the effects of nucleotide binding. Science. 2011; 334(6054):380–385. [PubMed: 22021858]
22. Barrera NP, Zhou M, Robinson CV. The role of lipids in defining membrane protein interactions: insights from mass spectrometry. Trends Cell. Biol. 2013; 23(1):1–8. [PubMed: 22980035]
23. Morgner N, Montenegro F, Barrera NP, Robinson CV. Mass spectrometry--from peripheral proteins to membrane motors. J. Mol. Biol. 2012; 423(1):1–13. [PubMed: 22750574]
24. Bush MF, et al. Collision cross sections of proteins and their complexes: a calibration framework and database for gas-phase structural biology. Anal. Chem. 2010; 82(22):9557–9565. [PubMed: 20979392]
25. Zhong Y, Hyung SJ, Ruotolo BT. Characterizing the resolution and accuracy of a second-generation traveling-wave ion mobility separator for biomolecular ions. Analyst. 2011; 136(17): 3534–3541. [PubMed: 21445388]
26. Shvartsburg AA, Smith RD. Fundamentals of traveling wave ion mobility spectrometry. Anal. Chem. 2008; 80(24):9689–9699. [PubMed: 18986171]
27. Giles K, et al. Applications of a travelling wave-based radio-frequency-only stacked ring ion guide. Rapid. Commun. Mass Spectrom. 2004; 18(20):2401–2414. [PubMed: 15386629]
28. Nagamatsu Y, Takeda K, Kuranaga T, Numoto N, Miki K. Origin of asymmetry at the intersubunit interfaces of V1-ATPase from Thermus thermophilus. J. Mol. Biol. 2013; 425(15):2699–2708. [PubMed: 23639357]
29. Suhre K, Sanejouand YH. ElNemo: a normal mode web server for protein movement analysis and the generation of templates for molecular replacement. Nucleic Acids Res. 2004; 32(Web Server issue):W610–614. [PubMed: 15215461]
30. Drory O, Frolow F, Nelson N. Crystal structure of yeast V-ATPase subunit C reveals its stator function. EMBO Rep. 2004; 5(12):1148–1152. [PubMed: 15540116]
31. Lee LK, Stewart AG, Donohoe M, Bernal RA, Stock D. The structure of the peripheral stalk of Thermus thermophilus H+-ATPase/synthase. Nat. Struct. Mol. Biol. 2010; 17(3):373–378. [PubMed: 20173764]
32. Bernal RA, Stock D. Three-dimensional structure of the intact Thermus thermophilus H+-ATPase/synthase by electron microscopy. Structure. 2004; 12(10):1789–1798. [PubMed: 15458628]
33. Stewart AG, Lee LK, Donohoe M, Chaston JJ, Stock D. The dynamic stator stalk of rotary ATPases. Nat. Commun. 2012; 3:687. [PubMed: 22353718]
34. Kinosita K Jr. Yasuda R, Noji H, Adachi K. A rotary molecular motor that can work at near 100% efficiency. Philos. Trans. R. Soc. Lond., Ser. B: Biol. Sci. 2000; 355(1396):473–489. [PubMed: 10836501]
35. Esteban O, Christ D, Stock D. Purification of molecular machines and nanomotors using phage-derived monoclonal antibody fragments. Methods Mol. Biol. 2013; 996:203–217. [PubMed: 23504426]
36. Arai S, et al. Rotation mechanism of Enterococcus hirae V1-ATPase based on asymmetric crystal structures. Nature. 2013; 493(7434):703–707. [PubMed: 23334411]
37. Giles K, Williams JP, Campuzano I. Enhancements in travelling wave ion mobility resolution. Rapid. Commun. Mass Spectrom. 2011; 25(11):1559–1566. [PubMed: 21594930]
38. Pagel K, Natan E, Hall Z, Fersht AR, Robinson CV. Intrinsically disordered p53 and its complexes populate compact conformations in the gas phase. Angew. Chem. Int. Ed. Engl. 2013; 52(1):361–365. [PubMed: 22777995]
39. Armbruster A, et al. Evidence for major structural changes in subunit C of the vacuolar ATPase due to nucleotide binding. FEBS Lett. 2005; 579(9):1961–1967. [PubMed: 15792803]
40. Lau WC, Rubinstein JL. Subnanometre-resolution structure of the intact Thermus thermophilus H +-driven ATP synthase. Nature. 2012; 481(7380):214–218. [PubMed: 22178924]

41. Beis I, Newsholme EA. The contents of adenine nucleotides, phosphagens and some glycolytic intermediates in resting muscles from vertebrates and invertebrates. Biochem. J. 1975; 152(1):23–32. [PubMed: 1212224]

42. Schneider DA, Gourse RL. Relationship between growth rate and ATP concentration in Escherichia coli: a bioassay for available cellular ATP. J. Biol. Chem. 2004; 279(9):8262–8268. [PubMed: 14670952]

43. Tani K, et al. Visualization of two distinct states of disassembly in the bacterial V-ATPase from Thermus thermophilus. Microscopy (Oxf). 2013; 62(4):467–474. [PubMed: 23572213]

44. Armbruster A, et al. Structural analysis of the stalk subunit Vma5p of the yeast V-ATPase in solution. FEBS Lett. 2004; 570(1-3):119–125. [PubMed: 15251451]

45. Hernandez H, Robinson CV. Determining the stoichiometry and interactions of macromolecular assemblies from mass spectrometry. Nat. Protoc. 2007; 2(3):715–726. [PubMed: 17406634]

46. van der Spoel D, et al. GROMACS: fast, flexible, and free. J. Comput. Chem. 2005; 26(16):1701–1718. [PubMed: 16211538]

47. Hess B, Bekker H, Berendsen HJC, Fraaije JGEM. LINCS: A linear constraint solver for molecular simulations. J. Comput. Chem. 1997; 18(12):1463–1472.

48. Reimann CT, Velazquez I, Tapia O. Proteins in vacuo. Denaturation of highly-charged lysozyme studied by molecular dynamics simulations. J. Phys. Chem. B. 1998; 102(46):9344–9352.

Europe PMC Funders Author Manuscripts

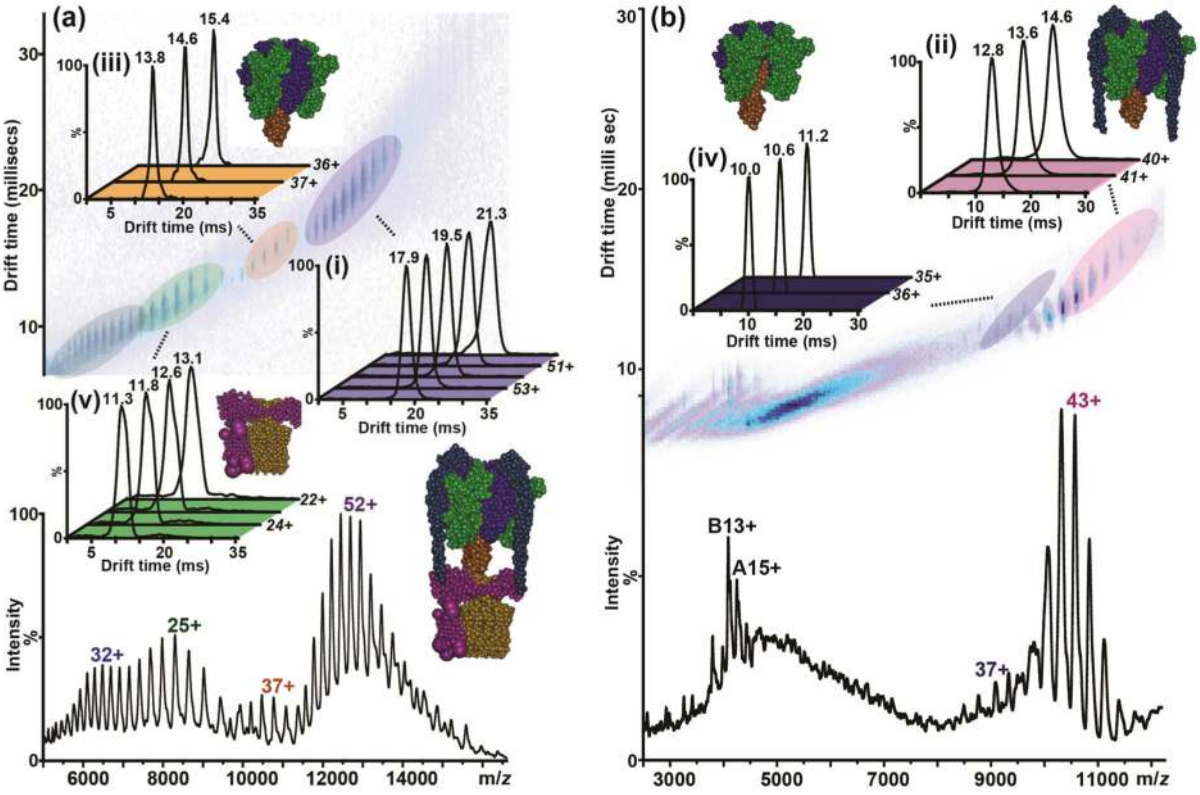

Figure 1. Flexibility of intact *Tt*ATPase and its subcomplexes assessed by IM-MS

2D IM-MS spectra showing the separation of ions according to their m/z ratios and mobility drift times recorded for different *Tt*ATPase species. (a) Extracted ATD contours are shown for charge state peaks for the intact complex (blue, i), solution disassembled V_1 (orange, ii) and V_o (green, iii), as well as (b) for the entire soluble domain V_1' (pink, iv) and the A_3B_2DF subcomplex (dark blue, v). The V_o series resulting from gas phase dissociation is not considered here (grey circle centred around 6000 m/z in a). Structural models of species (i)-(v) used for CCS calculation (Table 1) are shown in space-filling representations (see Supplementary Methods for details of model building).

Europe PMC Funders Author Manuscripts

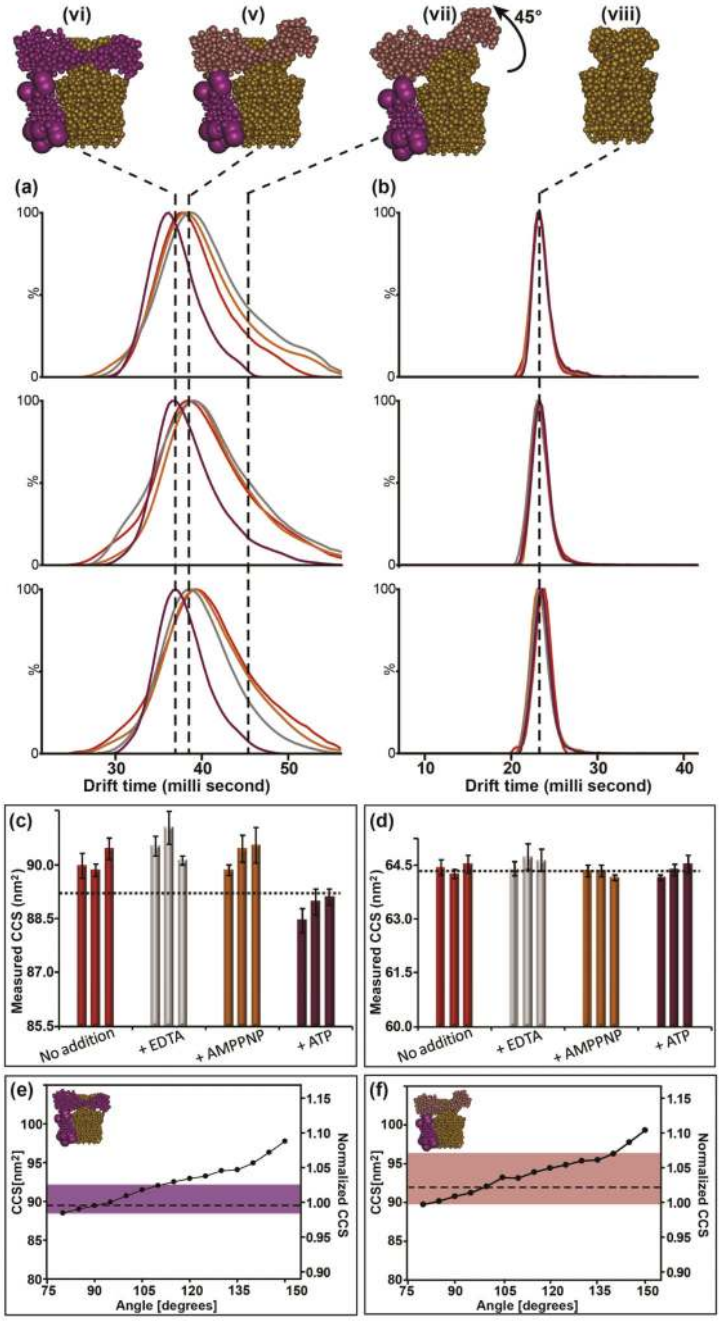

Figure 2. CCS measurements for the *Tt*ATPase ICL_{12} (V_o) and CL_{12} subcomplexes in different *Tt*ATPase preparations

(a,b) Extracted ATD peaks for the charge state 29+ of V_o (a) and 23+ of CL_{12} (b). Top row, purifications from cells harvested at stationary phase at pH 6.8, pH 8.2 (middle) and at log phase at pH 8.2 (bottom). Aliquots of *Tt*ATPase purified without additives were used as references and are coloured red; those with EDTA, AMPPNP or ATP are coloured grey, orange and purple respectively. Dashed lines indicate calculated arrival times for structural models of ICL_{12} incorporating I_{sol} (purple, vi) and I_{sol}' (pink, iii) in a horizontal position, I_{sol}' flexing upward by 45°(vii) as well as CL_{12} (viii). (c,d) CCS values averaged over four

sets of measurements for ICL_{12} (c) and CL_{12} (d) with standard deviations shown as error bars. The colours are the same as in (a,b). The dashed lines represent theoretical CCS calculated for the ICL_{12} (c) and CL_{12} (d) structural models. (e,f) CCS values calculated for structural models (vi and iii) of ICL_{12} are plotted against varying angles of I_{sol} with I_{mem} in the presence (e) and absence (f) of ATP, respectively. Experimental CCS and variations are represented by dashed lines and shaded areas, respectively.

Europe PMC Funders Author Manuscripts

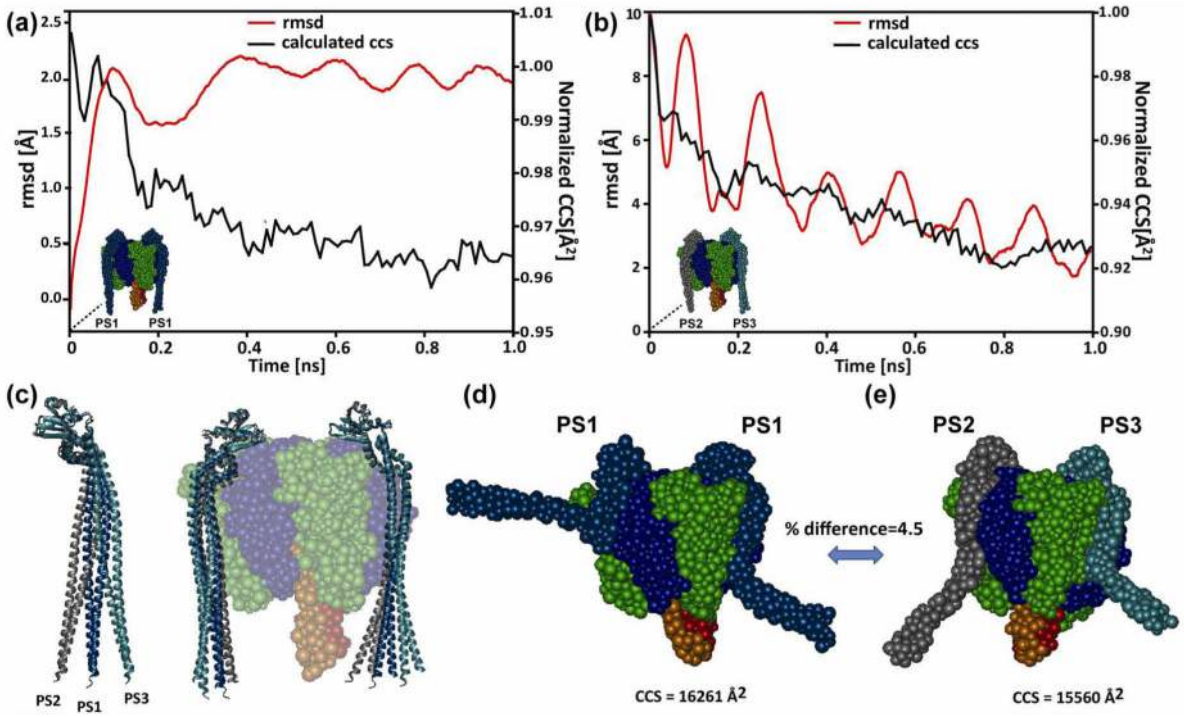

Figure 3. In vacuo molecular dynamics simulations of the catalytic head (V_1') of *Tt*ATPase

(a,b) A trajectory is depicted over 1 ns simulation with constant temperature (300 K) for the head V_1' starting with two different conformations of the peripheral stalks (insets). The average charge state (43+) observed from MS experiments was used to assign the charge distributions over the surface accessible basic residues (Supplementary Fig. S5). An RMSD-based clustering analysis was carried out and CCS calculated for structures along the simulation trajectory was plotted against the simulation time (red and black lines respectively). (c) Structural models of V_1' incorporating peripheral stalks in different conformations give a maximum difference of 1026 $Å^2$ in calculated CCS (see SI for details of model building). (d,e) Representative structures of both trajectories in the second 0.5ns simulation courses are displayed with a CCS difference of 4.5%. During the simulation the positions of the subunits within the core (V_1) are conserved, whereas the arms, representing the peripheral stalks, exhibit high flexibility consistent with CCS measurements.

Europe PMC Funders Author Manuscripts

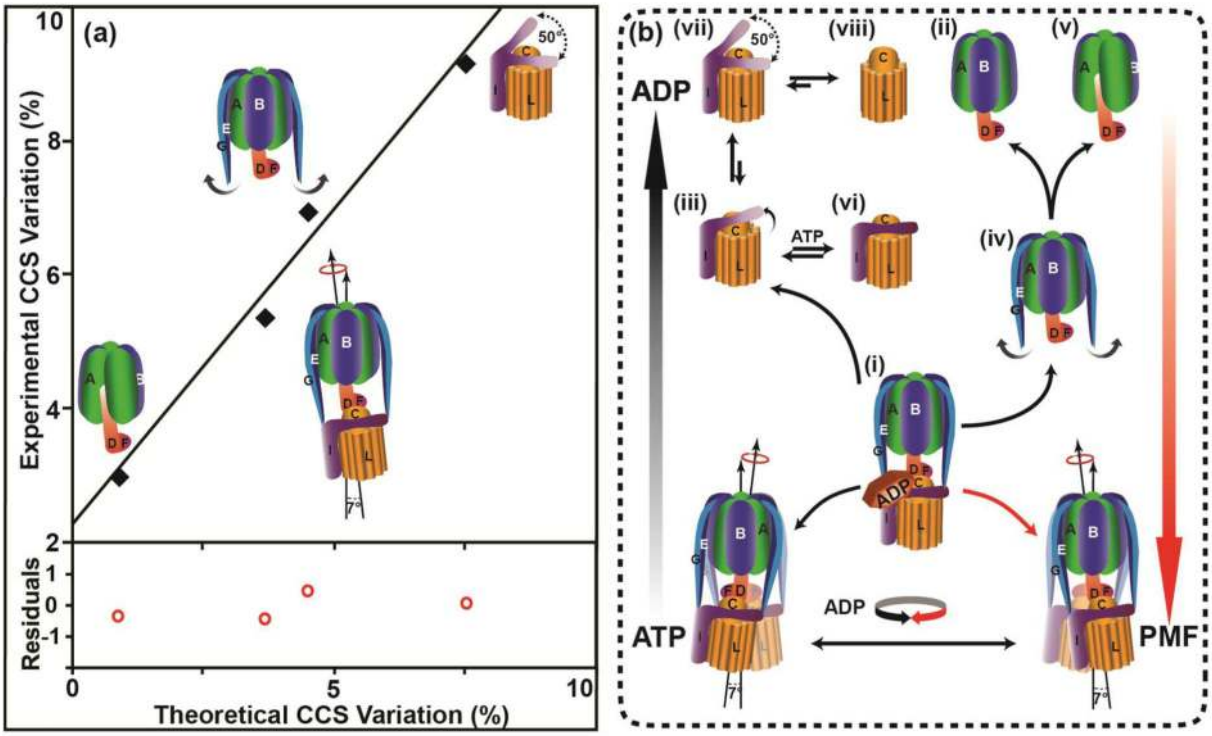

Figure 4. Nucleotide associated regulatory mechanism established by IM-MS

(a) Correlation of experimental with theoretical CCS variations calculated for conformational heterogeneity of different *Tt*ATPase species. Uncertainty of the measurement is shown at the bottom. (b) Regulatory mechanism proposed for *Tt*ATPase in response to unfavourable cellular conditions: deprivation of ATP and transmembrane proton motive force (PMF) results in ADP binding to allosteric sites in the complex (i), which is otherwise maintained by ATP or PMF operating for proton pumping or ATP synthesis (black and red arrows), respectively. ADP binding to the hinge region of subunit I in V_o triggers a conformational change converting I_{sol} (purple) to I_{sol}' (pink), destabilising its interaction with stator stalks and leading to disassembly of the intact complex. Flexibility of the stator components is evident in the ATD broadness observed for the two subcomplexes V_o (iii) and V_1' (iv), which could further dissociate to give subcomplexes (ii, v and viii). Increased CCS variation of V_o is consistent with dynamics of I_{sol}' within an angle of 50° (vii) eventually causing dissociation of I, a means suggested to silence proton translocation across the membrane (viii). ATP was demonstrated to be able to restore the active conformation of isolated V_o by restricting the mobility of the I_{sol} (vi) priming it for re-assembly.

Table 1

IM Resolution and CCS Values Measured for Intact *Tt*ATPase and its Subcomplexes

***Tt*ATPase species**	**Drift time Resolution (R_t)**	**Cross section resolution (R_Ω)**	**Experimental CCS (nm^2)**	**CCS Variation (%)**	**Theoretical CCS (nm^2)**
$\mathbf{V_oV_1}$ ($A_3B_3DFE_2G_2ICL_{12}$)	8.0	18.5	216 ± 2.1	5.4 ± 0.9	215
$\mathbf{V_o}$ (ICL_{12})	4.3	10.8	90 ± 1.9	9.2 ± 0.7	89
$\mathbf{CL_{12}}$	9.1	30.4	64 ± 1.3	3.3 ± 0.6	64
$\mathbf{V_1}$(A_3B_3DF)	14.2	34.6	138 ± 1.5	2.9 ± 0.5	137
$\mathbf{V_1'}$($A_3B_3DFE_2G_2$)	5.7	14.3	172 ± 2.0	7.0 ± 1.0	173
A_3B_2DF	13.3	33.8	135 ± 2.5	3.0 ± 0.8	133

Europe PMC Funders Author Manuscripts

Table 2

Measured CCS of ICL_{12} (V_o) and CL_{12} Subcomplexes in Different *Tt*ATPase Preparations

Sample ID	CCS_{ICL12} (nm^2)	% CCS Variation	CCS_{CL12} (nm^2)	% CCS Variation
14	90.0	8.1	64.4	2.3
10	90.5	9.0	64.4	2.5
23	89.9	8.7	64.3	2.1
19	88.4	6.6	64.2	2.3
13	89.8	9.2	64.2	2.4
11	91.0	10.6	64.7	2.2
22	90.4	9.2	64.3	2.1
18	89.0	6.3	64.4	2.2
16	90.4	9.0	64.5	2.2
12	90.1	8.1	64.6	2.4
24	90.5	8.3	64.2	2.3
20	89.1	6.3	64.5	2.2

Europe PMC Funders Author Manuscripts

Table 3

*Tt*ATPase Preparations under Different Conditions

Sample ID	Cell growth stage	Buffer pH	EDTA	AMP-PNP	ATP	Concentration (mg/mL)
10	Stationary phase	6.8	5mM	—	—	14.5
11	Stationary phase	8.2	5mM	—	—	13.9
12	Log phase	8.2	5mM	—	—	10.2
13	Stationary phase	8.2	—	—	—	13.3
14	Stationary phase	6.8	—	—	—	8.7
16	Log phase	8.2	—	—	—	5.7
18	Stationary phase	8.2	—	—	1mM	9.0
19	Stationary phase	6.8	—	—	1mM	7.2
20	Log phase	8.2	—	—	1mM	10.1
22	Stationary phase	8.2	—	1.9mM	—	13.3
23	Stationary phase	6.8	—	1.9mM	—	8.7
24	Log phase	8.2	—	1.9mM	—	5.7